Turbulent kinetic energy balance as a tool for estimating vertical diffusivity in wind-forced stratified waters

Alfred Wüest,[1] *Gabriel Piepke, and David C. Van Senden*
Swiss Federal Institute of Environmental Science and Technology (EAWAG), CH-8600 Dübendorf, Switzerland

Abstract

Based on microstructure measurements in a simply shaped lake basin, the sources of vertical mixing in the stratified part of the water body were identified and estimates of their relative importance obtained by balancing turbulent kinetic energy introduced by the wind. It was found that (1) ~1.9% of the vertical wind energy flux P_{10} (~39 mW m^{-2}), estimated 10 m above the lake surface, was available for turbulent mixing in the entire lake water body; (2) ~1.5% of P_{10} was dissipated by turbulence in the weakly stratified surface layer (epilimnion ~6 m deep), and ~0.42% of P_{10} reached the stratified deep water (hypolimnion) as turbulent kinetic energy via internal seiching; (3) ~90% of the turbulent kinetic energy in the stratified water (i.e., 0.38% of P_{10}) was dissipated within the bottom boundary layer of a few meters thickness, whereas only ~10% was lost in the interior (away from the boundary; 0.04% of P_{10}); and (4) as a consequence mixing within the bottom boundary was found to be the main source of vertical mixing for the deep waters of the whole lake. The ratio of buoyancy flux to dissipation (i.e., the mixing efficiency) was found to be $\gamma_{mix} \approx 0.15$, leading to agreement between the Osborn–Cox microstructure diffusivities and basin-wide tracer diffusivities.

Comparison with turbulent kinetic energy balances, performed in five other lakes, demonstrates that this analysis is representative for many enclosed water bodies, as long as wind is the dominant source of turbulent energy (i.e., if other processes, such as convective mixing, double diffusion, or riverine intrusions can be neglected). Although the lakes under consideration were very different in size and shape and although the currents in Lake Baikal were inertial rather than seiching related as in the other lakes, the turbulent kinetic energy balance was very similar and the mixing efficiency was identical. Typically, $0.3 \pm 0.1\%$ of P_{10} is transferred as turbulent kinetic energy into the stratified part of the water body, and $0.04 \pm 0.02\%$ of P_{10} is stored as potential energy in the stratification. This analysis provides a tool for estimating vertical diffusivity for wind-driven hypolimnetic mixing within a factor of two based on stratification and wind measurements alone.

Diapycnal exchange (perpendicular to surfaces of equal density) in stratified natural waters is of great importance both for its ecological implications and its relevance to environmental fluid dynamics. From a practical viewpoint, physically sound parameterizations of diapycnal diffusivity (usually synonymous with vertical diffusivity in enclosed basins) provide a robust basis for vertical mass flux estimates. Because diapycnal exchange in stable stratification requires energy, which is the fundamental source of mixing, turbulent kinetic energy (TKE) balancing can be used as an ideal alternative to estimating rates of mixing from tracer observations. The strength of the TKE approach lies in its foundation on energy conservation, a first principle of physics, and its potential for generalization of the results from laboratory to aquatic systems of different scales.

The link between TKE and mixing is the buoyancy flux $K_d N^2$ (W kg^{-1}) that expresses the rate of change of potential energy due to turbulent diffusion K_d (m^2 s^{-1}) in a stratified water column of stability N^2 (s^{-2}). Buoyancy flux is generally a small fraction, γ_{mix} (the so-called mixing efficiency), of the rate of energy transfer from large-scale currents to the smallest scales of motion (providing TKE), before the energy is eventually converted into heat by viscosity at the rate of dissipation ϵ (W kg^{-1}). This relationship may be used to estimate the diapycnal diffusivity (Osborn and Cox 1972; Osborn 1980):

$$K_d = \gamma_{mix} \epsilon N^{-2} \qquad \text{(m}^2\text{ s}^{-1}) \qquad (1)$$

Application of Eq. 1 is not as straightforward as it might seem: While the stability N^2 can routinely be determined from standard CTD profiles (conductivity, temperature, and depth), estimation of TKE dissipation ϵ requires an enormous effort, and γ_{mix} that depends both upon the physical processes (Ivey and Imberger 1991) and system properties such as topography and stratification (Gloor et al. 2000) is the bulk manifestation of complex processes. However, given knowledge of how much wind energy enters the water column and how this energy is distributed internally, the TKE balance provides a useful tool with which to derive diffusivity from readily measured parameters (such as wind and stratification).

To determine the TKE balance and to relate dissipation to tracer-based diffusivities, a set of measurements including wind, temperature microstructure, CTD, and thermistor profiles, as well as a tracer spreading experiment were made in
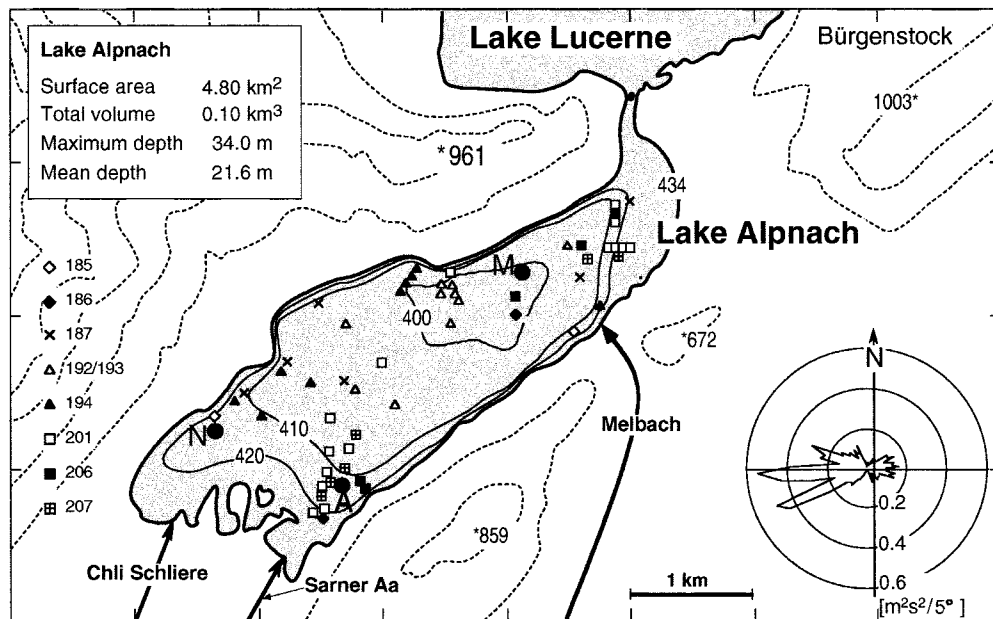
Fig. 1.   Map of Lake Alpnach (latitude: 47°N; longitude: 8°20′E) and surroundings: Depth contours, lake surface elevation, and heights of nearby mountains (asterisks) are given in m a.s.l. Thermistor strings (black dots), consisting of 11 sensors, were located at A (length 20 m), M (30 m), and N (15 m). The locations of the temperature microstructure profiles were scattered over the entire lake (symbols mark the profiles collected during the indicated day of the year). The inset gives the distribution of the square of the wind speed in angular sections of 5° (in the direction of the wind) at M, where the meteorological buoy was moored. Adapted from Münnich et al. (1992).

a medium-sized, freshwater basin during a 1-month stratified summer period. In particular the goals of the experiment were to: (1) quantify diapycnal diffusivities and compare direct estimates from microstructure measurements with indirect estimates inferred from tracers; (2) quantify the energy flux in the compartments of the water body (distribution of TKE dissipation); (3) identify the sources for production of potential energy (buoyancy flux); and (4) quantify the fractions of the turbulent wind energy flux used in mixing.

To avoid unnecessary complication in the estimation of the TKE and tracer balances, the experiment was conducted in a not-too-large lake. Lake Alpnach (Fig. 1) was considered to be an ideal site, due to its simple shape (nearly elliptical without special topographic features, surface area 4.8 km²), and the fact that the daily wind energy input during summer provides a significant source of TKE to the lake. Wind was the only driving force generating turbulence in the stratified hypolimnion, because during the period of the experiment (June/July 1989), the only relevant inflow enters the surface water from the warm surface of a higher elevation lake. Therefore, no intrusions into the stratified water body affect our balances of turbulence and heat. The stability, N^2 (Fig. 2), of the water column was solely temperature dependent (salinity: ~0.3‰) with relatively high values reflecting the strong stratification: $N^2 = g\rho^{-1}\partial\rho/\partial z \approx 10^{-5}–10^{-3}$ s⁻² (g, acceleration due to gravity; ρ, pressure-compensated density; z, depth, positive downward, $z = 0$ at surface).

TKE dissipation was determined from 130 temperature microstructure profiles, purposefully measured throughout the entire lake area (Fig. 1). The rate of change of the po-

tential energy was inferred from the heat budget that was calculated from continuously (every 10 min) recording thermistors at locations A, N, and M (Fig. 1) and from 82 CTD profiles, collected along the lake axis. The potential energy in the internal motion was estimated from internal seiche displacements derived from the isotherm depth records. Meteorological variables were monitored at M (Fig. 1). In addition an artificial tracer (SF_6) was released in the central part of the lake at 17 m depth (Wüest et al. 1996).

The interpretation and evaluation of this data set was supported by companion and subsequent studies of internal seiching (Münnich et al. 1992), bottom boundary layer dynamics and its effect on mixing (Gloor et al. 1994, 2000), the comparison of tracer- and microstructure-based diffusivity (Wüest et al. 1996), the quantification of interior and bottom boundary mixing by deliberately released artificial tracer (Goudsmit et al. 1997), and the effect of near-sediment stratification on the mixing efficiency (Wüest and Gloor 1998).

Observations

Wind energy flux—Wind speed and direction was measured at 10-min intervals, 4.5 m above the water surface ($W_{4.5}$) near the center of the lake (site M in Fig. 1) on a buoy-mounted Aanderaa meteorological station. In summer, atmospheric thermals produced by solar heating along the mountain slopes stimulate a diel wind blowing parallel to the lake's major axis (inset Fig. 1), with a pronounced max-
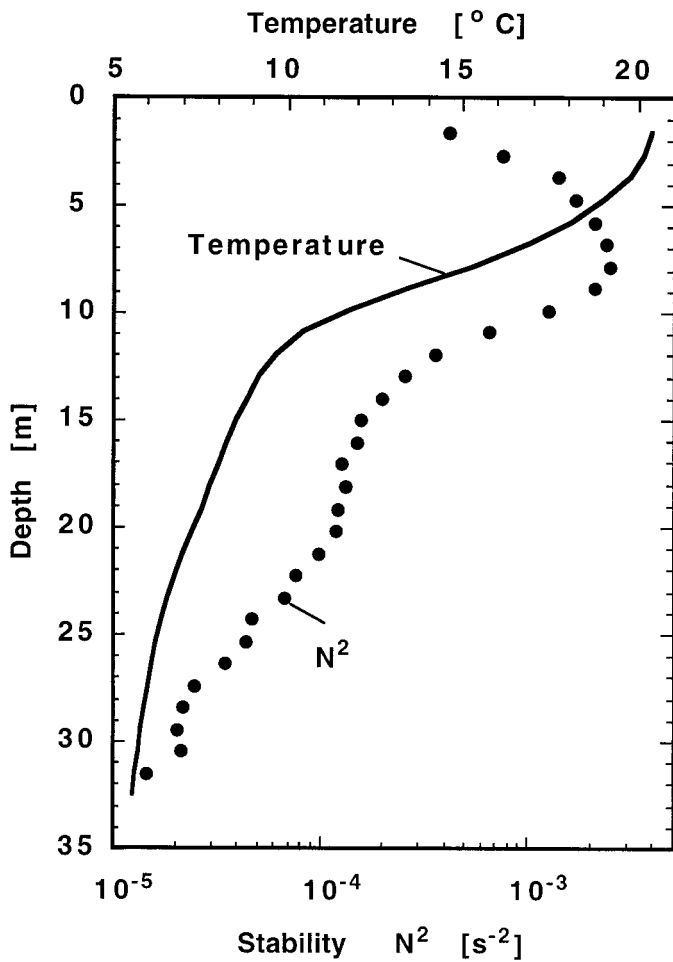
Fig. 2. Water column stability N^2 averaged over the 82 CTD profiles recorded during the 1-month study (June/July 1989). The temperature profile, showing the diel average of 28 June 1989, is representative, because vertical mixing did not change the vertical structure much during the study.
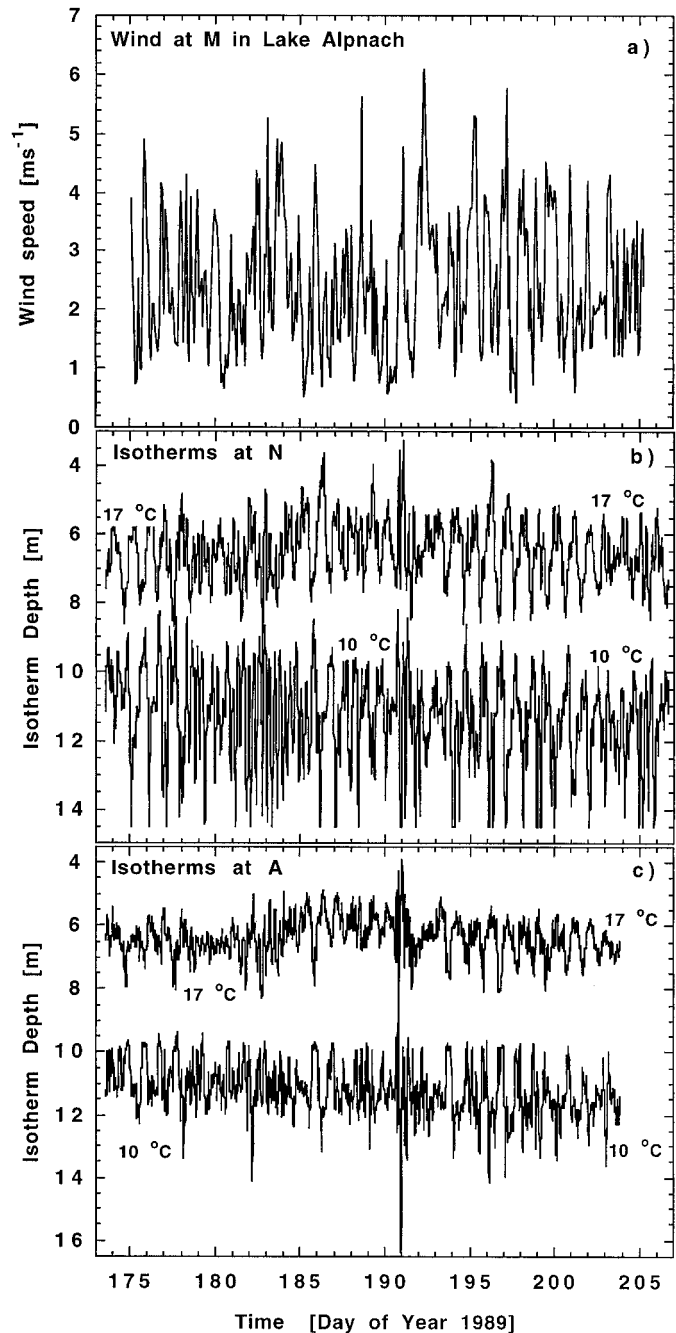

Fig. 3. (a) Two-hour averages of wind speed, measured at the meteorological station M (Fig. 1). The wind shows a regular diurnal pattern, peaking during afternoon. (b) Time series of the 10 and 17°C isotherm depths, calculated from the thermistor string at mooring N. The campaign-averaged vertical displacement $\langle d'^2 \rangle^{1/2} = 0.9$ and 1.4 m for the 10 and 17°C isotherms, respectively. (c) As b at mooring A. $\langle d'^2 \rangle^{1/2} = 0.64$ and 1.2 m for the 10 and 17°C isotherms, respectively. Two main periodicities of ~8 and ~24 h represent the first and second vertical seiche mode, respectively (details in Münnich et al. 1992).

imum in the afternoon (from ENE) and a weak maximum during the night (from WSW). In addition, on four occasions the diurnal wind was accompanied by strong westerlies (e.g., thunderstorms from WSW) that are typical for that time of the year in the region (Münnich et al. 1992).

The persistent wind applies regular forcing to the stratified water column and energizes the internal seiche modes. Spigel and Imberger (1980) demonstrated that one quarter of the period of the first horizontal and first vertical seiche mode (here ~8 h) is the most relevant for the transfer of momentum into the hypolimnion. Therefore the 10-min wind speed data were averaged over 2 h before further analysis (Fig. 3a), thereby removing the gusts that reached up to 12 m s^{-1}. After rescaling $W_{4.5}$ to W_{10}, the wind speed at standard 10 m height above water (Table 1), the average (indicated by $\langle \ \rangle$) wind speeds over the entire 1-month study period and over the nine microstructure profiling episodes were $\langle W_{10} \rangle \approx$ 2.7 m s^{-1} and ≈ 2.2 m s^{-1}, respectively.

The readily derived vertical turbulent wind energy flux 10 m above the lake surface (Lombardo and Gregg 1989),

$$P_{10} = \rho_{air} C_{10} W_{10}^3 \qquad (\text{W m}^{-2}) \qquad (2)$$

is used throughout the paper as a reference scale for the TKE input into the lake water (ρ_{air}, air density; $C_{10} \approx 0.9 \times 10^{-3}$, drag coefficient). Averages for the entire 1-month study pe-

Table 1. Turbulent kinetic energy balance in Lake Alpnach.

Energy flux/dissipation	Symbol/equation	mW m^{-2}	% of P_{10}
Flux from the atmosphere			
Entire 1-month study	$P_{10}^{\text{1-month}}$	39*	100
At time of microstructure casts	$P_{10}^{\text{MS-casts}}$	32*†	100
Surface boundary layer (SBL)			
Dissipation of TKE	$P_S = \rho \int_0^{6m} \langle \epsilon \rangle(z)\ dz$	0.47	1.5‡
	$P_S = \rho \int_{\delta_\nu}^{6m} \epsilon_{\text{LOW}}(z)\ dz = \rho u_{*S}^3 \ln\left(\frac{6m}{\delta_\nu}\right)$	0.51§	
Molecular viscous dissipation	$11\rho u_{*S}^3$	0.32§‖	
Total dissipation of SBL	$P_S + 11\rho u_{*S}^3$	0.79	2.5‡
Bottom boundary layer (BBL)			
Dissipation of TKE	$P_B = \rho \int_{\delta_\nu}^{10m} \epsilon_{\text{LOW}}(h)\ dh = \rho u_{*b}^3 \ln\left(\frac{10m}{\delta_\nu}\right)$	0.15¶	0.38#
Molecular viscous dissipation	$11\rho u_{*b}^3$	0.09‖	
Total dissipation in BBL	$P_B + 11\rho u_{*b}^3$	0.24	0.6#
Hypolimnion interior			
	$P_I = \frac{\rho}{A_{6m}} \int_{h=10m}^{z=6m} \langle \epsilon \rangle(z')A(z')\ dz'$	0.015**	0.04#
Hypolimnion basin-wide			
Total dissipation in hypolimnion	$P_B + 11\rho u_{*b}^3 + P_I$	0.26	0.67#
Turbulent dissipation in hypolimnion	$P_B + P_I$	0.17	0.42#
Storage of potential energy	$P_{\text{pot}} = \frac{\rho}{A_{6m}} \int_{\text{max depth}}^{6m} N^2(z)K_T(z)A(z)\ dz$	0.024	0.06#
Lake (entire water body)			
Total dissipation in the lake	$P_S + 11\rho u_{*s}^3 + P_I + P_B + 11\rho u_{*b}^3 + P_{\text{pot}}$	1.24	3.2††
Turbulent dissipation in the lake	$P_S + P_I + P_B + P_{\text{pot}}$	0.74	1.9††

* $W_{4.5m}$, wind measured 4.5 m above water, was rescaled to W_{10m} (for the standard height of 10 m) using LOW (logarithmic wind profile) and assuming a smooth flow with a standard roughness length of $0.1\nu/u_{*s}$ (i.e., multiply $W_{4.5m}$ by a factor of 1.07).
† Microstructure profiles were collected on the dates 185, 186, 187, 192, 193, 194, 201, 206, 207.
‡ Scaled to $P_{10}^{\text{MS-casts}} = 32$ mW m^{-2}.
§ Surface boundary layer: $u_{*s} = 3.1$ mm s^{-1} and $\delta_\nu = 11\nu/u_{*s}$.
‖ Calculated from $\nu(\partial u/\partial z)^2$ in the viscous sublayer (Imboden and Wüest 1995).
¶ Bottom boundary layer: $u_{*b} = 2.0$ mm s^{-1} and $\delta_\nu = 11\nu/u_{*b}$.
# Scaled to $P_{10}^{\text{1-month}} = 39$ mW m^{-2}.
** Integration in the interior excluding SBL ($z = 6$ m) and BBL ($h = 10$ m).
†† $P_S + 11\rho u_{*s}^3$ rescaled to $P_{10}^{\text{1-month}}$.

riod and for the microstructure profiling episodes were $\langle P_{10} \rangle \approx 39$ mW m^{-2} ($\langle W_{10}^3 \rangle^{1/3} \approx 3.1$ m s^{-1}) and 32 mW m^{-2} ($\langle W_{10}^3 \rangle^{1/3} \approx 3.0$ m s^{-1}), respectively (Table 1).

Internal seiches—The response of the stratified hypolimnion to the regular wind forcing is shown in Fig. 3b,c for the 10°C and 17°C isotherms at locations A and N. Spectral analysis of the isotherm time series revealed two dominant periodicities that correspond to the first vertical/first horizontal and second to the vertical/first horizontal seiche modes (Münnich et al.

1992). In-situ current data are not available for this study; however, subsequent measurements have shown that the bottom currents along the major axis of the lake (amplitude typically varying from 3 to 6 cm s^{-1}) correlate perfectly with the vertical displacements of the hypolimnetic isotherms for both modes (Gloor et al. 1994). In addition, Münnich (1996) applied a topography-dependent seiche model and demonstrated that for the simple basin and stratification structure of Lake Alpnach the horizontal hypolimnetic currents were generally rectilinear and showed negligible lateral variation.

Internal seiches contain kinetic and potential energy that are the intermediate reservoirs linking wind energy input to hypolimnetic TKE production. The kinetic energy, due to the seiche-related currents, and the potential energy, given by the vertical displacement $d(z)$ of the isotherms relative to their equilibrium positions z (Fig. 3b,c) in the stratification N^2 (Fig. 2) are interrelated by the seiching motion. The total internal seiche energy E_{IS} is the sum of both the potential and the kinetic energy. Because both averages are identical, E_{IS} is equal to two times the average potential energy, which itself is given by the vertical isotherm displacements $d(z)$. Assuming the two positions A and N are representative for the potential energy, then E_{IS} is determined by integrating over the entire hypolimnion (Munk 1981) and yields a campaign-average of

$$E_{IS} = \frac{\rho}{A_{surface}} \int_{max\ depth}^{surface} N^2(z)\langle d^2(z)\rangle A(z)\ dz$$

$$\approx 22 \pm 3\ \text{J m}^{-2}. \quad (3)$$

Dissipation—Vertical profiles of dissipation ϵ of TKE were determined using Batchelor's method, which is based on the fact that small-scale temperature fluctuations are always present in natural waters. Under isotropic and stationary conditions the one-dimensional spectrum of the temperature fluctuations, at the smallest spatial scales ($\sim$mm), is given by (Batchelor 1959; Gibson and Schwarz 1963)

$$\phi_T(k_z) = \frac{\pi\chi\kappa_T^{1/2}q^{3/2}\nu^{3/4}}{\epsilon^{3/4}}\left\{\frac{e^{-y^2}}{y} - \sqrt{\pi}[1 - \text{erf}(y)]\right\}$$

$$(\text{K}^2\ (\text{cpm})^{-1}) \quad (4)$$

where k_z (cpm) denotes the vertical one-dimensional wavenumber, $y = 2\pi k_z\kappa_T^{1/2}\nu^{1/4}q^{1/2}\epsilon^{-1/4}$ is the nondimensional wavenumber, $\kappa_T \approx 1.4 \times 10^{-7}$ m^2 s^{-1} the thermal molecular diffusivity, ν (1–1.5 $\times$ 10^{-6} m^2 s^{-1}) the kinematic viscosity, and $q \approx 3.4$ the experimentally determined turbulence parameter (Grant et al. 1968; Dillon and Caldwell 1980; Oakey 1982; Imberger and Boashash 1986). Rates of dissipation of TKE, ϵ (W kg^{-1}), and of temperature variance, χ (K^2 s^{-1}), were determined by fitting Batchelor's model spectrum ϕ_T to the spectra calculated from measured temperature profile segments.

One hundred and thirty such temperature microstructure casts were taken on nine occasions during July 1989 using a self-contained profiler (Carter and Imberger 1986) freely rising at about 0.1 m s^{-1} from 0.4 m above the sediment. Data were collected at 100 Hz from a pair of FP-07 fast-response thermistors and transmitted via an extrathin electrical cable to an on-board computer. After filtering and response time correction (Fozdar et al. 1985), the temperature microstructure profiles were divided into turbulent and non-turbulent segments (Imberger and Ivey 1991) before spectral analysis. Temperature spectra that did not follow Batchelor's form of Eq. 4 ($<$10% of the segments) were excluded from further analysis. The error introduced due to ambiguous spectra is far below the statistical uncertainty of $\sim$20% for vertically integrated dissipation.
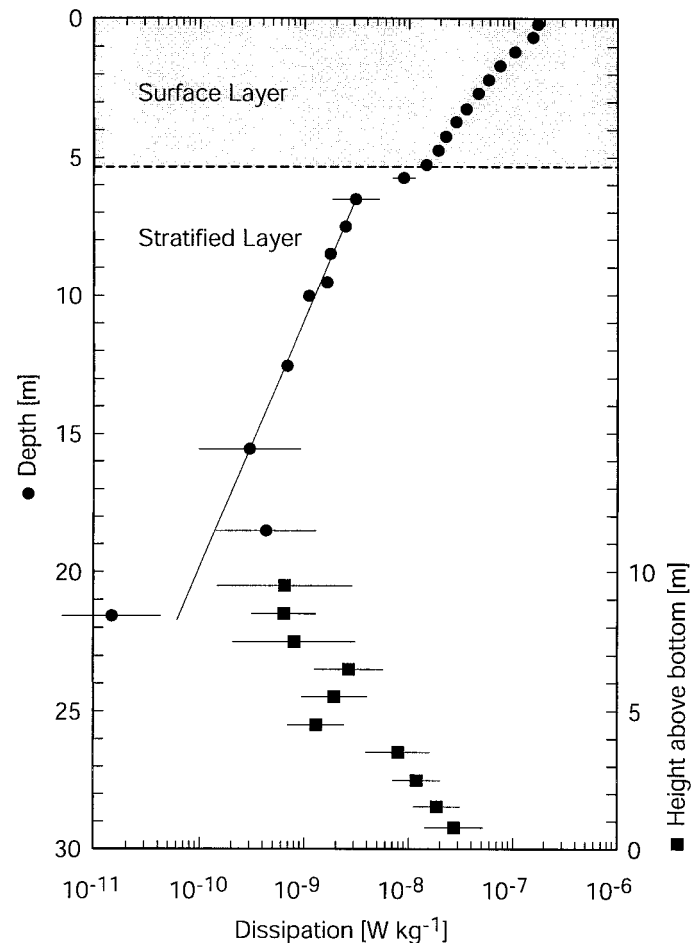
The 130 dissipation profiles extended from the surface

Fig. 4. Campaign-averaged arithmetic means of dissipation $\langle \epsilon \rangle$, averaged in vertical depth bins ($\langle \epsilon(z)\rangle$, left scale; dots) and in bins above the sediment ($\langle \epsilon(h)\rangle$; right scale; squares). The error bars represent the 95% confidence interval, estimated with the bootstrap method. The shading refers to the SBL. The line indicates the z-dependent exponential decrease in the upper hypolimnion.

(uprising sensor) to the local depth, according to the topography (Fig. 1). Dissipation—generally decreasing with depth—increased substantially above the lake sediment (at all sites), indicating two different sources of TKE production in the stratified body, namely, the surface and the bed. In order to quantify the two processes separately, the dissipation profiles were averaged in two different ways: (1) Averaging in depth bins, beginning at the surface and extending downward to 10 m above the local lake bottom (i.e., to a maximum of 24 m, which is 10 m above maximum lake depth), enabled campaign-averaged dissipation in the interior to be obtained (Fig. 4, left scale); (2) dissipation estimates in the bottom boundary were campaign-averaged for height bins starting at 0.5 m above the local lake bottom and extending upward (Fig. 4, right scale).

For averaging in predefined bins individual dissipation estimates were weighted by the segment length assuming zero dissipation outside the turbulent segments. For the campaign averages $\langle \epsilon(z)\rangle$, the bootstrap error estimate of $\langle \epsilon(z)\rangle$ (Efron

and Gong 1983) and the intermittency (standard deviation of $\langle \ln[\epsilon(z)] \rangle$; (Baker and Gibson 1987) were calculated.

Surface layer dissipation: The campaign-averaged dissipation $\langle \epsilon(z) \rangle$ decreased rapidly as a function of depth z, closely following an exponential decay (2.8×10^{-7} W kg^{-1} exp$^{-[z/1.7\text{ m}]}$), before dropping off at $\sim 5.5 \pm 0.5$ m depth (Fig. 4). Within the margin of intermittency, $\langle \epsilon(z) \rangle$ decreased in the top few meters inversely proportional to depth, implying Law of the Wall (LOW) scaling for ϵ (Dillon et al. 1981; Lombardo and Gregg 1989)

$$\epsilon_{\text{LOW}}(z) = \frac{u_{*S}^3}{kz} \qquad (\text{W kg}^{-1}) \qquad (5)$$

where $k = 0.41$ is von Kàrmàn's constant. Fitting Eq. 5 to $\langle \epsilon(z) \rangle$ (Fig. 4) yields a surface friction velocity of $\langle u_{*S}^3 \rangle^{1/3} \approx$ 3.1 mm s^{-1}, characterizing the surface boundary layer (SBL) turbulence. Comparing u_{*S} with the wind during microstructure measurements ($\langle W_{10}^3 \rangle^{1/3} \approx 3.0$ m s^{-1}) allows the surface drag coefficient that is commonly used in the bulk parameterization $\langle u_{*S}^3 \rangle^{1/3} = (\rho_{\text{air}} C_{10m}/\rho)^{1/2} \times \langle W_{10}^3 \rangle^{1/3}$ to be estimated. The resulting drag coefficient $C_{10m} \approx 0.9 \times 10^{-3}$ fits well within the range of low wind speed estimates (Amorocho and deVries 1980; Bradley et al. 1991; Wu 1994). Although this relationship implies that the production of turbulence in the SBL is proportional to $\langle W_{10}^3 \rangle$ (Oakey and Elliott 1982; Imberger 1985), there is not sufficient data to allow a detailed analysis of the temporal and vertical response of ϵ to wind.

Turbulence data were collected during the daytime when convection was absent and the SBL stably stratified. The stability N^2 ranged from 10^{-4} to 10^{-3} s^{-2} in the SBL, increasing at ~ 5 to 6 m depth where dissipation dropped off. Above this depth (primarily defined by nighttime cooling) the water column was turbulent for most of the time, indicated by the criterion for active turbulence,

$$\epsilon > 20\nu N^2 \qquad (\text{W kg}^{-1}) \qquad (6)$$

(Stillinger et al. 1983; Rohr et al. 1987; Gibson 1986, 1991). In the top 5 m the campaign-average $\langle \epsilon(z) \rangle$ was larger than the campaign-average $20\nu\langle N^2(z) \rangle$ and subsequently the turbulent eddies overcame the suppressing effects of viscosity ν and stability N^2 at the eddy overturning scale $(\epsilon N^{-3})^{1/2}$ (Dillon 1982) in the 10s of cm range. This is corroborated by the output of the segmentation algorithm (Imberger and Ivey 1991) that was applied to the temperature microstructure data. At the surface $\sim 80\%$ of the profiles were identified as turbulent while the percentage dropped off sharply at ~ 5.5 m depth. At 6 m depth only $\sim 20\%$ of the profiles showed turbulent segments.

Interior hypolimnion dissipation: Within the intrinsic scatter, dissipation also decayed exponentially in the stratified interior ($\langle \epsilon(z) \rangle \sim$ exp$^{-[z/4.0\text{ m}]}$), although with a slower rate (Fig. 4). Starting at the top of the hypolimnion (6 m depth) with $\langle \epsilon(6\text{m}) \rangle \approx 3.6 \times 10^{-9}$ W kg^{-1}, dissipation $\langle \epsilon(z) \rangle$ decreased to the detection limit (some 10^{-11} W kg^{-1}) at about 20 m depth. This rapid decrease is most probably due to lower interior shear at greater depth and is to be expected for the two observed dominant vertical seiche modes. Also

the turbulent fraction of segments fell quickly and reached $\sim 1\%$ at the deepest interior site (~ 24 m depth). Consistently, the overturning scale of potential eddies shortened to the mm to cm range, where viscosity suppresses such small eddies. Consequently, the activity criterion, $\epsilon > 20\nu N^2$, was never attained by the observed $\langle \epsilon(z) \rangle$ within the interior hypolimnion.

Bottom boundary dissipation: By contrast to the interior, dissipation within the bottom boundary layer (BBL), averaged in height bins, increased significantly while approaching the sediment (Fig. 4, right scale). Again, within the margin of the natural variability and in accordance with the LOW (Dewey and Crawford 1988; Thorpe 1988), $\langle \epsilon(h) \rangle$ increased proportionally to h^{-1} (h, height above local bottom), within a few meters of the bottom but deviated from the h^{-1} behavior at distances exceeding 5–10 m above bottom. The thickness of the well-mixed BBLs is assumed to be the result of a competition between the background stratification N^2 (at the considered depth), suppressing turbulence and reducing the BBL, and the bottom currents, generating turbulence and expanding the BBL. Based on this reasoning, Gloor et al. (2000) developed a simple model that could reproduce the BBL thickness of a few meters reasonably well. Comparing $\langle \epsilon(h) \rangle$ with $20\nu N^2$ shows indeed that for $h < 7$ m, the activity criterion (Eq. 6) was well satisfied (again at eddy overturning scales of several dm), whereas above the BBL turbulence became increasingly sporadic on entering the nonturbulent interior.

Fitting LOW scaling (Eq. 5) to $\langle \epsilon(h) \rangle$ in Fig. 4 yields a BBL friction velocity of $u_{*b} \approx 2.0$ mm s^{-1} that corresponds to a typical current speed of $(C_{1m})^{-1/2} \cdot u_{*b} \approx 4$–5 cm s^{-1} at 1 m above bottom, depending on whether $C_{1m} \approx 1.6 \times 10^{-3}$ (Elliott 1984) or $C_{1m} \approx 2.2 \times 10^{-3}$ (Ravens et al. 2000) is used for the drag coefficient. This current speed is typical of the seiche-related deep-water currents at that time of the season (Gloor et al. 1994).

Vertical diffusivity—Temperature-based vertical diffusivity K_T (m^2 s^{-1}) was determined in the stratified water below 6 m depth by the heat budget method (Powell and Jassby 1974) that was applied to the temperature data from the continuously recording Aanderaa thermistor strings at A and N (Fig. 1; string at M failed after 10 d) and to the 82 CTD profiles (collected on eight occasions during the experiment). The diffusivity estimate is based on the assumption that at depth z, the vertical turbulent transport of heat, $\rho c_p K_T(z) A(z) \partial T(z)/\partial z$ is equal to the rate of change of heat content below that depth, given by

$$\int_{\text{max depth}}^{z} \rho c_p A(z') \frac{\partial T(z')}{\partial t} \, dz',$$

where $A(z')$ is the lake plan area at depth z', and c_p is the specific heat. Equating these two terms gives for the vertical diffusivity

$$K_T(z) = \left[A(z) \frac{\partial T(z)}{\partial z} \right]^{-1} \int_{\text{max depth}}^{z} A(z') \frac{\partial T(z')}{\partial t} \, dz' \qquad (\text{m}^2 \text{ s}^{-1}).$$

$$(7)$$

Temporal gradients $\partial T(z')/\partial t$ were estimated from thermistor data in the depth range of the strings and from CTD profiles below the thermistors. The CTD profile enabled accurate determination of the vertical gradients $\partial T(z)/\partial z$ in the near-bottom zone.

Vertical diffusivity $K_T(z)$ (Fig. 5) was determined as a campaign-average (from end June to end July 1989) by applying Eq. 7 to the entire temperature data set (CTD and thermistor strings). K_T did not vary much as a function of depth: In the main part of the hypolimnion K_T was estimated as 0.03–0.04 cm² s⁻¹, in excellent agreement with the SF₆ tracer-based estimate (Fig. 5). K_T was slightly higher in the deepest layers and decreased to a minimum of ~0.01 cm² s⁻¹ at the top of the hypolimnion. The error, which depends mainly on the uncertainty of $\partial T(z)/\partial t$ (and to a lesser extent on the uncertainty of $\partial T(z)/\partial z$), is largest at maximum depth, where the temporal gradient of T is not well defined and decreases to negligible values at the upper end (Fig. 5). Although it may appear evident, it is important to notice that both temperature- and tracer-based diffusivities represent basin-wide estimates, averaging over all mixing processes occurring within the basin at the respective depth, whereas microstructure-based estimates capture only the turbulence that is crossing the path of the profiler in the interior of the water body.

Turbulent kinetic energy balance in the lake water body

In this section, the volume-integrated dissipation (Table 1) is given for the SBL, the stratified interior, the BBL, and for the hypolimnion as a whole.

Surface layer dissipation—Based on the vertical structure of ϵ and N^2 and the arguments on the turbulence activity, the thickness of the SBL is estimated at 6 m. The integrated turbulent dissipation within the SBL is given by

$$P_S = \rho \int_0^{6\text{m}} \langle \epsilon \rangle(z) \, dz \approx 0.47 \text{ mW m}^{-2}. \quad (8a)$$

Note that this value depends only weakly on the integration method (Table 1). Integrating Eq. 5 up to the viscous sublayer of the SBL (thickness: $\delta_\nu \approx 11\nu/u_{*S} \approx 3.5$ mm) and using $u_{*S} \approx 3.1$ mm s⁻¹ leads to almost identical integrated turbulent dissipation of

$$P_S = \rho \int_{\delta_\nu}^{6\text{m}} \epsilon_{\text{LOW}}(z) \, dz = \rho u_*^3 \ln\left(\frac{6\text{m}}{\delta_\nu}\right)$$

$$\approx 0.51 \text{ mW m}^{-2}. \quad (8b)$$

Although the molecular dissipation within the viscous sublayer (Schlichting 1968), given by $11\rho u_{*s}^3 \approx 0.32$ mW m⁻² (Table 1), occurs as a nonturbulent process and is therefore irrelevant for mixing, it is the total loss of energy that affects the kinetic energy balance and thereby the damping of the physical system (Imboden and Wüest 1995). The total SBL dissipation in the open water region of the lake (sum of turbulent plus viscous) is therefore ~0.79 mW m⁻², which
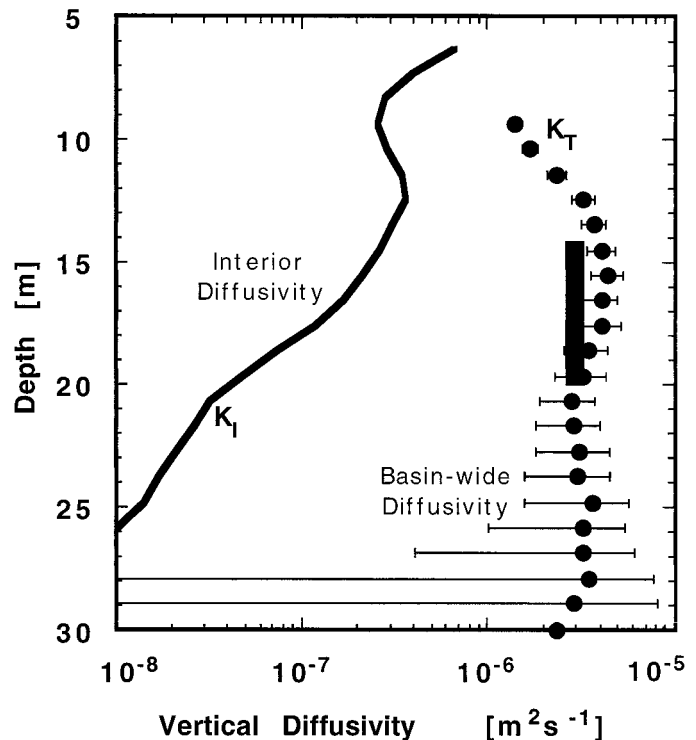

Fig. 5.   Basin-wide vertical diffusivity determined by the heat budget (K_T; black dots) and by SF₆ (black square) compared to diapycnal diffusivity K_I in the interior (solid line) determined by the microstructure measurement.

is ~2.5% of the wind energy flux P_{10}, at the times of microstructure measurements (Table 1). Of the total SBL dissipation, about 60% (1.5% of P_{10}) can be attributed to dissipation of TKE (Table 1). This dissipation however would significantly overestimate the apparent residence time scale of mechanical energy in the surface layer, because even in medium–large lakes a significant amount of the energy is transferred by waves to the shore.

Dissipation in the interior—The area-specific turbulent dissipation in the interior of the hypolimnion is given by the vertical integral from $h \approx 10$ m above bottom to $z \approx 6$ m depth:

$$P_I = \frac{\rho}{A_{6\text{m}}} \int_{h=10\text{m}}^{z=6\text{m}} \langle \epsilon \rangle(z') A(z') \, dz' \approx 0.015 \text{ mW m}^{-2}. \quad (9)$$

Because the layer volume decreases substantially with depth we include the depth-dependent lake plan area $A(z')$. The turbulent energy dissipation in the hypolimnion interior is very small and amounts to only 0.04% of P_{10} (Table 1). The molecular dissipation ($\nu[\partial u/\partial z]^2$) is at least an order of magnitude smaller and therefore neglected.

Dissipation in the BBL—Corresponding to the LOW, the integration of Eq. 5 with $u_{*b} \approx 2.0$ mm s⁻¹ over the entire logarithmic BBL from the viscous sublayer $\delta_\nu \approx 11\nu/u_{*b}$ to the logarithmic layer thickness $\delta_B \approx 10$ m yields the turbulent BBL dissipation of

$$P_B = \rho \int_{\delta_\nu}^{\delta_B} \epsilon_{\text{LOW}}(h) \; dh = \frac{\rho}{k} u_{*b}^3 \ln(\delta_B/\delta_\nu)$$

$$\approx 0.15 \text{ mW m}^{-2}. \tag{10}$$

The choice of the thickness δ_B of the temporally varying BBL is not crucial to the estimate of Eq. 10: Taking $\delta_B \approx 5$ m would reduce the integral by $<10\%$, which is smaller than what is considered as a realistic relative error (the absolute error of the method may be larger; Kocsis et al. 1999). The molecular dissipation within the viscous sublayer, $11\rho u_{*b}^3 \approx 0.09$ mW m^{-2} (Table 1) again adds to the total BBL dissipation of $P_B + 11\rho u_{*b}^3 \approx 0.24$ mW m^{-2} (corresponding to $\sim 0.6\%$ of P_{10}), which is the relevant energy loss for damping the hypolimnetic currents and energy.

Storage of potential energy in the stratification—The rate of change of potential energy of the stratification in the hypolimnion was determined by calculating the buoyancy flux $K_T N^2$ (W kg^{-1}), which expresses the irreversible change of the potential energy, as the result of turbulent diapycnal diffusion of density against the stability. The integrated rate of change of potential energy in the hypolimnion has been calculated according to

$$P_{\text{pot}} = \frac{\rho}{A_{6\text{m}}} \int_{\text{max depth}}^{6\text{m}} N^2(z) K_T(z) A(z) \; dz$$

$$\approx 0.024 \; (\pm 0.003) \text{ mW m}^{-2} \tag{11}$$

where for K_T the temperature-based basin-wide diffusivity (Fig. 5) and for N^2 the campaign-average stability (Fig. 2) has been applied. Comparison with the wind energy input shows that only $\sim 0.062\%$ of P_{10} was ultimately irreversibly stored as potential energy.

Summary—The TKE budget for the entire lake, as well as for the SBL, the BBL, and the hypolimnion are summarized in Table 1. From the vertical energy flux at 10 m above lake level $\sim 3.2\%$ of the vertical wind energy flux P_{10} entered the lake water body and $\sim 1.9\%$ of P_{10} became available for turbulent mixing. A large fraction of the energy, as much as $\sim 2.5\%$ of P_{10}, remained in the SBL, whereas $\sim 0.7\%$ of P_{10} leaked into the stratified hypolimnion. As little as $\sim 0.4\%$ of P_{10} became available for turbulent mixing and only $\sim 0.06\%$ of P_{10} was irreversibly stored in the stratification.

Significance of TKE budget for hypolimnetic mixing

Temporal dynamics of mixing—The residence time of the hypolimnetic internal mechanical energy is given by the seiche energy E_{IS} (Eq. 3) divided by the total dissipation in the hypolimnion. The campaign-averaged values of E_{IS} (~ 22 J m^{-2}; Table 2) and the total hypolimnetic dissipation ($P_B + 11\rho u_{*b}^3 + P_I \approx 0.26$ mW m^{-2}; Table 1), respectively, lead to a residence time of $E_{IS}/(P_B + 11\rho u_{*b}^3 + P_I) \approx 1$ d. Because most of the seiche energy that scales proportional to u_{*b}^2 is dissipated in the BBL, where $\epsilon \sim u_{*b}^3 \sim E_{IS}^{3/2}$, the residence time (proportional to E_{IS}/ϵ) scales as $u_{*b}^{-1} \sim E_{IS}^{-1/2} \sim \epsilon^{-1/3}$ (Gloor et al. 2000). As a consequence, the seiche energy in the hypolimnion relaxes on a short time scale after strong

excitation (fig. 21 in Imboden and Wüest 1995), whereas in weakly energized hypolimnia, internal seiche energy can reside for long periods of time (Lemmin 1987). This result implies that strongly energized hypolimnia can only be observed for short periods after forcing, whereas weakly excited hypolimnetic currents will reside for longer periods and are almost always observable.

The mechanical energy reservoir in the hypolimnion is proportional to the volume, whereas dissipation is proportional to the sediment area (almost equal to the lake surface area). Subsequently the damping time scale of the internal seiches is also approximately proportional to the average hypolimnion depth. This is consistent with observations from the ocean (depth: 3,800 m; $\tau \sim 90$ d; Gregg and Sanford 1988), Lake Baikal south basin (depth: 1,400 m; $\tau \sim 40$ d; Ravens et al. 2000), Lake Ueberlingen (depth: 147 m; $\tau \sim 3$ d; Schimmele 1993), Sempachersee (depth: 87 m; $\tau \sim 2$ d; Wüest 1987), and this study (depth: 34 m; $\tau \sim 1$ d), indicating that the residence time is on average about 1 d per 38 m of water depth (0.026 d m^{-1}).

Mixing efficiency—The portion γ_{mix} of the dissipated TKE (i.e., $P_B + P_I$ in the stratified water) is turned over to potential energy P_{pot} and irreversibly stored in the stratification as a result of mixing. The estimation of both, P_{pot} (~ 0.024 mW m^{-2}; Eq. 11) and $P_B + P_I$ (~ 0.165 mW m^{-2}; Table 1), allows the mixing efficiency to be determined by $\gamma_{\text{mix}} = P_{\text{pot}}/(P_B + P_I) \approx 0.15$ for this particular water body (Table 1). In general, the mixing efficiency depends not only on the physics of shear-induced turbulence (Ivey and Imberger 1991) but also on site-specific factors, such as the vertical structure of the stratification, especially in the BBL, where the mixing efficiency drops (Wüest and Gloor 1998; Gloor et al. 2000). Because here most of the hypolimnion was stratified, $\gamma_{\text{mix}} \approx 0.15$ is representative for other stratified natural waters subject to shear turbulence. This value is indeed well within the variation found in the ocean (Gregg 1987; Peters and Gregg 1988; Ivey and Imberger 1991; Gargett and Moum 1995) and in Lake Baikal (Ravens et al. 2000).

Vertical diffusivity—The mixing efficiency γ_{mix} allows the vertical diffusivity in the stratified hypolimnion to be determined on the basis of the TKE balance. Applying the average turbulent hypolimnetic dissipation $\epsilon_{\text{hypo}} \approx 9 \times 10^{-9}$ W kg^{-1} (Table 2) and stratification $N^2 \approx 4.5 \times 10^{-4}$ s^{-2} to Eq. 1 leads to an average diapycnal diffusivity of $K_d \approx 0.030$ cm^2 s^{-1} (Table 2). Over a large section of the hypolimnion, this average value is in excellent agreement with the vertical diffusivities inferred from the heat budget (Fig. 5; Table 2) and from the spreading of artificially introduced SF$_6$ (Fig. 5; Table 2). Both tracer-based estimates represent basin-wide diffusivities, because temperature and SF$_6$ sense the entire extent of the water body along particular isopycnals. It is concluded that the Osborn–Cox (1972) model, underlying Eq. 1, is an adequate method for determining tracer-independent diffusivities, based purely on the TKE balance within the considered water body.

Because only $\sim 10\%$ of the hypolimnetic internal seiche energy was dissipated in the interior of the stratified water body ($\epsilon_I \approx 9 \times 10^{-10}$ W kg^{-1}; Table 2), the average interior

Table 2. Experiment averages of turbulence-relevent quantities in the hypolimnion (>6 m depth) of Lake Alpnach (June/July 1989).

Quantity	Value	Reference
Internal seiche energy	$E_{IS} \approx 22 \pm 3$ J m^{-2}	Eq. 3
Total dissipation	$P_B + P_I + 11\rho u_{*b}^3 \approx 0.26$ mW m^{-2}	Table 1
Energy residence time	$\tau_{IS} = E_{IS}/(P_B + P_I + 11\rho u_{*b}^3) \approx 1$ d	Table 1
Rate of change of potential energy	$P_{\text{pot}} \approx 0.024$ mW m^{-2}	Table 1; Eq. 11
Mixing efficiency	$\gamma_{\text{mix}} = P_{\text{pot}}/(P_B + P_I) \approx 0.145$	Table 1
Turbulent dissipation*	$\epsilon_{\text{hypo}} = (P_B + P_I)/(\rho H_{\text{hypo}}) \approx 9 \times 10^{-9}$ W kg^{-1}	Table 1
Interior dissipation*	$\epsilon_I = P_I/(\rho H_{\text{hypo}}) \approx 9 \times 10^{-10}$ W kg^{-1}	Eq. 9
Stability of stratification*	$N^2 \approx 4.5 \times 10^{-4}$ s^{-2}	Fig. 2
Diapycnal diffusivity†	$K_d = \gamma_{\text{mix}}\epsilon_{\text{hypo}}/N^2 \approx 2.9 \times 10^{-6}$ m^2 s^{-1}	Eq. 1
Temperature-based vertical diffusivity*	$K_T \approx 2.9 \times 10^{-6}$ m^2 s^{-1}	Eq. 7
Tracer-based vertical diffusivity‡	$3.0\ (\pm 0.4) \times 10^{-6}$ m^2 s^{-1}	Fig. 5
Interior diffusivity§	$K_I = \gamma_{\text{mix}}\epsilon_I/N^2 \approx 3 \times 10^{-7}$ m^2 s^{-1}	Eq. 1
Interior activity§	$\epsilon_I/(\nu N^2) \approx 1.5$	This table

* Volume-averaged below 6 m depth and using the average hypolimnion depth of $H_{\text{hypo}} \approx 18$ m.
† Calculated from the averages of γ_{mix}, ϵ_{hypo}, and N^2.
‡ In 17 m depth (vertical range 15–20 m), from Wüest et al. (1996).
§ Calculated from the averages of γ_{mix}, ϵ_I, and N^2.

diapycnal diffusivity $K_I = \gamma_{\text{mix}}\epsilon_I N^{-2} \approx 0.003$ cm^2 s^{-1} (Table 2) was also only ~10% of the basin-wide estimate. By contrast to the basin-wide diffusivity that was nearly constant in the hypolimnion, K_I varied strongly as a function of depth (Fig. 5), with a slight but clear minimum at ~8 m depth. This minimum coincides with the minimum vertical displacement of isotherms $\langle d'^2(z)\rangle^{1/2}$ (Fig. 3b,c) and the correspondingly larger gradient Richardson number associated with the second vertical seiche mode at that particular depth (Münnich et al. 1992). Below ~12 m depth, K_I decreased rapidly as a function of depth, falling below molecular diffusivity of heat, because the turbulence $\epsilon_I(z)$ (Fig. 4) faded out faster than the stability $N^2(z)$ (Fig. 2). The largest values of $K_I(z)$ appear at the top of the hypolimnion (bottom of the SBL), where TKE is produced by internal shear.

Also the rate of dissipation of temperature variance (Eq. 4), χ, was at least an order of magnitude smaller in the interior compared to the BBL (not shown). Correspondingly, the Thorpe scale (Thorpe 1977) that follows closely the overturning scale (Dillon 1982) was much smaller in the interior than in the BBL, where the Thorpe scale approaches the thickness of the well-mixed bottom layer.

Vertical transport of TKE—Consistent with these observations, a very rough a-posteriori TKE balance shows that the interior local TKE production ($\sim\epsilon_I$) was orders of magnitude larger than the divergence of the turbulent downward mixing of TKE ($\sim \partial[K_I\tau\partial\epsilon/\partial z]/\partial z$). Therefore, it is concluded that the rapid decline of $\epsilon_I(z)$ as a function of depth in the hypolimnion is due to the increasing gradient Richardson numbers, at greater depth, which is a property of the first as well as second vertical seiche mode (Münnich et al. 1992). The low diffusivity (less than molecular diffusivity of heat) at greater depths is consistent with its functional dependence on the gradient Richardson number, as observed by others (Peters et al. 1988).

The role of the BBL—The extremely low value of the interior diffusivity K_I was at first a surprising result that seemed inconsistent with the vertical diffusivity of the temperature budget method. However, by injecting tracer dye into the interior of the hypolimnion, Goudsmit et al. (1997) verified in a subsequent experiment that dissolved substances indeed diffuse in the interior as slow as K_I, the value inferred from the Osborn–Cox model-based (Eq. 1) microstructure measurements. The ratio of the basin-wide to interior diffusivities was found to be ~10 to 25 (depending on how the ratio was formed). As Fig. 6 shows, the ratio of the basin-wide diffusivity K_T (from heat budget, Fig. 5) to interior diffusivity K_I (Fig. 5) is indeed in that range and increases with depth.

The ratio of the basin-wide to interior dissipation shows the same feature. It is assumed that the BBL-related dissipation (P_B) is everywhere the same per unit area of sediment and therefore the volume-specific dissipation is proportional to $\partial A/\partial V$, the sediment area per water volume. At depth z, BBL-related dissipation is $(\partial A/\partial V)(P_B/\rho)$. The ratio of basin-wide to interior dissipation is then given by

$$\frac{\dfrac{\partial A}{\partial V}\dfrac{P_B}{\rho} + \epsilon_I(z)}{\epsilon_I(z)} = \frac{\dfrac{\partial A}{\partial V}\dfrac{u_{*B}^3}{k}\ln(\delta_B/\delta_\nu) + \epsilon_I(z)}{\epsilon_I(z)} \quad (-). \quad (12)$$

At the top of the hypolimnion, interior and BBL dissipations were comparable (ratio ~2) but already at mid-depth, where the tracer studies were performed (Goudsmit et al. 1997), the ratio was ~10–20 (Fig. 6). In the deepest part the ratio becomes very large, because $\partial A/\partial V$ increases and $\epsilon_I(z)$ decreases with depth. In the upper hypolimnion the diffusivity ratio K_T/K_I shows good agreement with the ratio of energy dissipation (Eq. 12) despite the large uncertainty. It becomes evident that the relative importance of boundary mixing
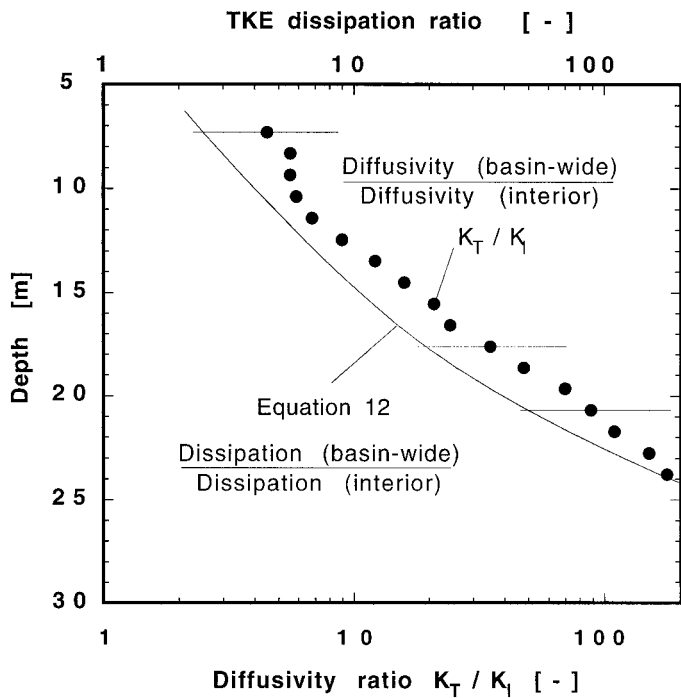
Fig. 6. Ratio of basin-wide diffusivity K_T (determined from heat budget) to interior diffusivity K_I as measured in this study (dots), compared to the ratio of basin-wide dissipation to interior dissipation (line), as calculated by Eq. 12.

Table 3. Transfer of turbulent kinetic and potential energy to the stratified hypolimnia of different lakes.

Lake	$(P_B + P_I)/P_{10}$ (10^{-3})	P_{pot}/P_{10} (10^{-3})	Reference
Lake Babine	1.9*	0.29†	Farmer and Carmack (1981)
Baldeggersee	—	0.31‡	Wüest (1987)
Sempachersee	—	0.14‡	
Urnersee	—	0.49‡	
Lake Baikal	1.8§‖	0.29¶	Ravens et al. (2000)
Baldeggersee (k-ε Modeling)	3.8‖#	0.56*	Goudsmit et al. (2000)
Lake Alpnach	4.2	0.61	This study
Average	2.9 ± 1.2	0.38 ± 0.17	

* Calculated based on $\gamma_{mix} = 0.15$.
† In Farmer and Carmack (1981) P_{pot} is given as $0.26\rho U_{*s}^3$. The ratio P_{pot}/P_{10} is subsequently given by $0.26(C_{10}\rho_{air}/\rho)^{1/2} = 0.00029$ for a value of $C_{10} = 0.001$.
‡ Episodes with different winds with different temporal scales were analyzed. Variations of P_{pot}/P_{10} were in Baldeggersee: 0.31 ± 0.26; Sempachersee: 0.14 ± 0.06; Urnersee: 0.49 ± 0.47.
§ The TKE balance indicated an energy transfer into the permanently stratified water of 0.22% of P_{10}, whereof interior as well as boundary mixing contributed to equal parts (Ravens et al. 2000).
‖ Forty percent of the boundary dissipation assumed to be molecular (Table 1).
¶ Calculated based on $\gamma_{mix} = 0.16$, as determined by mocrostructure measurements (Ravens et al. 2000).
# The model calculations revealed an energy transfer to internal seiching of 0.62% of P_{10}.

steadily increases with depth. The deviations at greater depths (not shown) are discussed in Gloor et al. (2000).

Rate of change of potential energy in other stratified waters

From a practical point of view, scientists and engineers are often interested in estimating diffusivities for a particular water body based on easy-to-measure parameters such as bathymetry, stratification, and wind exposure, without carrying out detailed field studies. In that respect it is of considerable practical importance to determine whether the TKE balance presented above is site specific or can be generalized. The following examples demonstrate that the relative amount of TKE available for mixing in the hypolimnion is a surprisingly constant fraction of the wind power P_{10}. In order to substantiate this generalization, we review and summarize those studies in stratified natural waters (in chronological order, Table 3) that address the flux of potential energy in relation to the wind power.

Lake Babine—Farmer and Carmack (1981) describe a winter-time investigation of the vertical deepening of the inverse temperature stratification that occurs when surface temperatures drop below the temperature of maximum density. Lake Babine, their study site, located in northern British Columbia (Canada), is a long, deep (maximum depth 235 m), narrow, and steep-sided basin. Near-homogeneous properties below the depth of temperature of maximum density indicate strong vertical hypolimnetic mixing that had been

attributed to wind-induced large-amplitude internal surges (Farmer 1978). Farmer and Carmack (1981) estimated the potential energy uptake needed to deepen the inverse temperature stratification and compared it with the vertical wind energy flux P_{10} (Eq. 2). They found that $0.26\rho u_{*s}^3$, which corresponds to 0.29×10^{-3} of P_{10} (Table 3) contributed to diapycnal mixing in the hypolimnion. Although the seven times deeper Lake Babine has a very different topography and density structure than Lake Alpnach, the mixing energy per wind input was the same, given the uncertainty of the estimates.

Three lakes in Central Switzerland—Using the heat budget method, basin-wide vertical diffusivities $K_T(z)$ were estimated in the three medium-sized lakes of Baldeggersee (1981; maximum depth: 66 m; area: 5.2 km²), Sempachersee (1982/83; 86 m; 14 km²), and Urnersee (1986; 196 m; 22 km²) for several summer periods (Wüest 1987). Stability $N^2(z)$ of the stratification was determined from large numbers of CTD profiles, including the freshwater salinity (important in Baldeggersee). Wind was again recorded from an Aanderaa meteo-buoy, moored in the centers of the lakes. In all three lakes, mixing is caused by wind-induced internal seiching. The rate of change of the potential energy of the stratification was calculated by vertically integrating $K_T(z)N^2(z)$ in the hypolimnion. Within the margin of error, the three energy fluxes (Table 3), $0.31 \times 10^{-3} \times P_{10}$ (Baldeggersee), $0.14 \times 10^{-3} \times P_{10}$ (Sempachersee), and $0.49 \times 10^{-3} \times P_{10}$ (Urnersee), were consistent with the values given above.

Lake Baikal south basin—In Lake Baikal wind was also identified as the driving force for diapycnal mixing in the permanently stratified hypolimnion. However, almost the entire kinetic energy was at the inertial scales, and seiching (except some spurious surging) was not considered an important component of the kinetic energy balance. In-situ turbulence measurements in the 1,390-m deep south basin, carried out in 1996/1997 showed that 2.2×10^{-3} of P_{10} arrived in the permanently stratified water body (Ravens et al. 2000) and 1.8×10^{-3} of P_{10} was dissipated through turbulence. Using 0.16 for the mixing efficiency, which has been determined in Lake Baikal by temperature microstructure profiles, yields again a rate of change of potential energy of $0.29 \times 10^{-3} \times P_{10}$ (Table 3), consistent with the previous estimates.

Baldeggersee—Continuous Aanderaa thermistor string data, recorded again in Baldeggersee during 1995/1996, were used to calibrate a k-ϵ model designed for mixing studies in lakes (Goudsmit, Burchard, Peeters, Reichert and Wüest pers. comm.). One of the two model parameters is the energy fraction of P_{10} entering the hypolimnion. It was found that 6.2×10^{-3} of P_{10} reached the hypolimnion and $3.8 \times 10^{-3} \times P_{10}$ dissipated through turbulence. Again, assuming a mixing efficiency of 0.15, as determined above (Table 1), yields a rate of change of potential energy of $0.56 \times 10^{-3} \times P_{10}$ (Table 3)—again well within the range of the other values.

Summary—Although the presented data have been gathered by completely different methods (heat budget, microstructure, turbulence modeling), the resulting fluxes of mixing energy are astonishingly coherent: $2.9 \pm 1.2 \times 10^{-3} \times P_{10}$ is found to dissipate as TKE and thereof an average rate of $0.38 \pm 0.17 \times 10^{-3} \times P_{10}$ (Table 3) gets stored as potential energy. This corresponds to an average mixing efficiency of 13% (0.38/2.9). From the six lakes considered here, only one (Sempachersee) deviated more than expected considering the uncertainty of such large-scale budget estimates. In addition, Lake Alpnach had a slightly more efficient energy transfer perhaps due to the shallow depth and the resonance of the second vertical seiche mode with the wind forcing. It is noteworthy that Lake Baikal has such a similar TKE budget, considering the lake's greater size and depth and considering the wind energy input was purely inertial rather than via seiche currents.

TKE balances in the ocean, where measurements and budgeting is much more difficult to complete, are rare. However, Denman and Miyake (1973), Kullenberg (1976), and Holloway (1980) estimated the mixing-related rates of change of the potential energy in the entire water column (including the surface layer) to 1.2×10^{-3}, 1.9×10^{-3}, and 2.1×10^{-3} times P_{10}, respectively. Considering that only about 10% (Lake Baikal) to 20% (Lake Alpnach) of the surface TKE production reaches the stratified water body below, these oceanic observations are surprisingly consistent with the values in Table 3.

In summary, it is concluded, that a robust estimate of the diapycnal diffusivity K_d can be derived from the wind energy flux P_{10} by

$$\frac{\rho}{A_{hypo}} \int_{\text{hypolimnion}} N^2(z) K_d(z) A(z) \, dz$$

$$\approx 0.38 \pm 0.17 \times 10^{-3} \times P_{10} \qquad (\text{W m}^{-2}). \quad (13)$$

Conclusions

Measurements, carried out in a small- to medium-scale lake enabled quantification of the TKE balance. After analyzing a 1-month period of measurements including 82 CTD profiles, 130 temperature microstructure profiles, 2 thermistor string records, wind record, and an artificial tracer release, the following conclusions can be drawn:

Using P_{10}, the turbulent energy flux at 10 m above water level, as a reference, it was found that 3.2% of P_{10} entered the lake and 1.9% of P_{10} became available for turbulent mixing. Most of the mechanical energy, entering the lake, dissipated in the SBL ($\sim$80%), whereas the minor part (20%) reached the strongly stratified hypolimnion.

Dissipation in the SBL decayed approximately exponentially with depth with a penetration scale of $\sim$1.7 m. The LOW may also be applicable but there were not sufficient data to test this. The dissipation levels indicate that most of the SBL was turbulent. The latter conclusion may not hold for extremely stratified SBLs, where turbulence is inhibited by stability.

In the interior of the hypolimnion turbulence also decayed exponentially with depth but with a longer depth scale of $\sim$4 m. Dissipation in the interior was a very small part of the TKE balance, contributing only 0.04% of P_{10}. Turbulence was weak ($\sim$1.5νN^2) and the microstructure profiles indicated that only a few % of the observed water column was turbulent, consistent with the fact that the activity level was an order of magnitude below active turbulence ($\sim$20νN^2), typical for the ocean interior (Gregg and Sanford 1988). Therefore, interior turbulent mixing was barely above molecular diffusivity of heat.

Within the BBL of 5–10 m thickness, dissipation increased toward the sediment, following the LOW. The BBL-integrated turbulent dissipation was found to be 0.4% of P_{10}, 10 times the interior dissipation. Assuming a classical boundary layer, this level of turbulence was consistent with the seiche-related deep water currents found in a subsequent experiment (Gloor et al. 1994).

Given a classical boundary layer, the residence time (τ) of the mechanical energy in the hypolimnion is inversely proportional to the internal seiche currents ($\tau \sim u^{-1}$). As a consequence, strongly excited seiches relax on a short time scale, whereas afterward, weak excitation can reside for weeks or months and hence is more likely to be observed.

These measurements revealed that hypolimnetic diapycnal mixing has two distinct sources: one in the interior (away from the boundary) and one within the BBL. On average, 90% of basin-wide diapycnal mixing may be attributed to bottom boundary mixing and the remaining 10% to locally produced turbulence in the interior. Indeed, in subsequent tracer experiments (Goudsmit et al. 1997), ratios of basin-wide to interior diffusivity of 10–25 were found. The ratios of both basin-wide to interior dissipation and diffusivity in-

crease with depth, because both the gradient Richardson number and the sediment surface area to volume ratio increase with depth.

These findings, consistent with observations in Mono Lake by MacIntyre et al. (1999), lead to the general conclusion that bottom boundary mixing is the dominant process for diapycnal transport in the hypolimnion of small- to medium-sized lakes. Recent measurements in Lake Baikal (Ravens et al. 2000) showed that dissipation in the permanently stratified water column (250 to ~1,400 m depth) was as large in the bottom boundary as in the interior, indicating the dominance of boundary mixing in deeper layers as well. This observation is also corroborated by results of tracer experiments in the ocean (Ledwell and Watson 1991; Ledwell et al. 1993; Toole et al. 1994), where interior diapycnal diffusivities, calculated from the vertical spread of tracer clouds, were also small compared to typical basin-wide diffusivity estimates. Ledwell and Bratkovich (1995) demonstrated that the vertical spread of a tracer increased rapidly when the tracer met the bottom boundaries of the basin (Ledwell and Hickey 1995). All these studies underline the role of bottom boundary mixing in stratified natural water diffusion.

Basin-wide diffusivities derived from tracers (temperature and SF_6) allow direct estimation of the rate of change of the potential energy of the stratification. Comparing this rate of change of the potential energy with the total dissipation in the hypolimnion results in a mixing efficiency of $\gamma_{mix} \approx 0.15$, which is typical of values determined in other strongly stratified natural waters.

Turbulence measurements as well as the basin-wide tracer balances led to the same net buoyancy flux, which expresses the net effect of diapycnal diffusivity in the stratified water column. This agreement demonstrates that the Osborn–Cox model is well suited for the determination of diffusivity based on the TKE balance, inferred from microstructure or inertial-subrange measurements.

The comparison of TKE balances, performed in five other lakes and in ocean basins, demonstrates that the fraction of TKE transferred to the stratified hypolimnion was similar for the very different enclosed water bodies. Although the lakes under consideration varied substantially in size and shape and although the currents in Lake Baikal were inertial rather than seiching related as in the other lakes, it was found that typically $0.3 \pm 0.1\%$ of the vertical wind energy flux P_{10} is transferred as turbulent kinetic energy into the deeper stratified part of the water body, and that $0.04 \pm 0.02\%$ of P_{10} was stored as potential energy in the stratification.

This analysis provides a tool to estimate diffusivity for wind-driven hypolimnetic mixing within a factor of two based on stratification and wind measurements alone.

References

AMOROCHO, J., AND J. J. DEVRIES. 1980. A new evaluation of the wind stress coefficient over water surfaces. J. Geophys. Res. **85:** 433–442.

BAKER, M. A., AND C. M. GIBSON. 1987. Sampling turbulence in the stratified ocean: Statistical consequences of strong intermittency. J. Phys. Oceanogr. **17:** 1817–1836.

BATCHELOR, G. K. 1959. Small-scale variation of convected quantities like temperature in turbulent fluid. Part 1. General discussion and the case of small conductivity. J. Fluid Mech. **5:** 113–133.

BRADLEY, E., P. COPPIN, AND J. GODFREY. 1991. Measurements of sensible and latent heat flux in the western equatorial Pacific Ocean. J. Geophys. Res. **96:** 3375–3389.

CARTER, G. D., AND J. IMBERGER. 1986. Vertically rising microstructure profiler. J. Atmos. Oceanic Technol. **3:** 462–471.

DENMAN, K. L., AND M. MIYAKE. 1973. Upper layer modification at Ocean Station Papa: Observations and simulation. J. Phys. Oceanogr. **3:** 185–196.

DEWEY, R. K., AND W. R. CRAWFORD. 1988. Bottom stress estimates from vertical dissipation rate profiles on the continental shelf. J. Phys. Oceanogr. **18:** 1167–1177.

DILLON, T. M. 1982. Vertical overturns: A comparison of Thorpe and Ozmidov length scales. J. Geophys. Res. **87:** 9601–9613.

———, AND D. R. CALDWELL. 1980. The Batchelor spectrum and dissipation in the upper ocean. J. Geophys. Res. **85:** 1910–1916.

———, J. G. RICHMAN, C. G. HANSEN, AND M. D. PEARSON. 1981. Near-surface turbulence measurements in a lake. Nature **290:** 390–392.

EFRON, B., AND G. GONG. 1983. A leisurely look at the bootstrap, the jackknife and cross-validation. Am. Statistician **37:** 36–48.

ELLIOTT, A. J. 1984. Measurements of the turbulence in an abyssal boundary layer. J. Phys. Oceanogr. **14:** 1779–1786.

FARMER, D. M. 1978. Observations of long nonlinear internal waves in a lake. J. Phys. Oceanogr. **8:** 63–73.

———, AND E. C. CARMACK. 1981. Wind mixing and restratification in a lake near the temperature of maximum density. J. Phys. Oceanogr. **11:** 1516–1533.

FOZDAR, F. M., G. J. PARKER, AND J. IMBERGER. 1985. Matching temperature and conductivity sensor response characteristics. J. Phys. Oceanogr. **15:** 1557–1569.

GARGETT, A. E., AND J. N. MOUM. 1995. Mixing efficiency in turbulent tidal fronts: Results from direct and indirect measurements of density flux. J. Phys. Oceanogr. **25:** 2583–2608.

GIBSON, C. H. 1986. Internal waves, fossil turbulence, and composite ocean microstructure spectra. J. Fluid Mech. **168:** 89–117.

———. 1991. Turbulence, mixing, and heat flux in the ocean main thermocline. J. Geophys. Res. **96:** 20,403–20,420.

———, AND W. H. SCHWARZ. 1963. The universal equilibrium spectra of turbulent velocity and scalar fields. J. Fluid Mech. **16:** 365–384.

GLOOR, M., A. WÜEST, AND D. M. IMBODEN. 2000. Dynamics of mixed bottom boundary layers and its implications for diapicnal transport in a stratified, natural water basin. J. Geophys. Res. **105:** 8629–8646.

———, ———, AND M. MÜNNICH. 1994. Benthic boundary mixing and resuspension induced by internal seiches. Hydrobiologia **284:** 59–68.

GOUDSMIT, G.-H., F. PEETERS, M. GLOOR, AND A. WÜEST. 1997. Boundary versus internal mixing in stratified natural waters. J. Geophys. Res. **102:** 27,903–27,914.

GRANT, H. L., B. A. HUGHES, W. M. VOGEL, AND A. MOILLIET. 1968. The spectrum of temperature fluctuations in turbulent flow. J. Fluid Mech. **34:** 423–442.

GREGG, M. C. 1987. Diapycnal mixing in the thermocline: A review. J. Geophys. Res. **92:** 5249–5286.

———, AND T. B. SANFORD. 1988. The dependence of turbulent dissipation on stratification in a diffusively stable thermocline. J. Geophys. Res. **93:** 12,381–12,392.

HOLLOWAY, P. E. 1980. A criterion for thermal stratification in a wind-mixed system. J. Phys. Oceanogr. **10:** 861–869.

IMBERGER, J. 1985. The diurnal mixed layer. Limnol. Oceanogr. **30:** 737–770.

———, AND B. BOASHASH. 1986. Application of the Wigner-Ville distribution to temperature gradient microstructure: A new technique to study small-scale variations. J. Phys. Oceanogr. **16:** 1997–2012.

———, AND G. N. IVEY. 1991. On the nature of turbulence in a stratified fluid, part II: Application to lakes. J. Phys. Oceanogr. **21:** 659–679.

IMBODEN, D. M., AND A. WÜEST. 1995. Mixing mechanisms in lakes, p. 83–138. *In* A. Lerman, D. M. Imboden, and J. Gat [eds.], Lakes: Chemistry, geology, physics. Springer.

IVEY, G. N., AND J. IMBERGER. 1991. On the nature of turbulence in a stratified fluid. Part I: The energetics of mixing. J. Phys. Oceanogr. **21:** 650–659.

KOCSIS, O., H. PRANDKE, A. STIPS, A. SIMON, AND A. WÜEST. 1999. Comparison of dissipation of turbulent kinetic energy determined by shear and temperature microstructure. J. Mar. Systems **21:** 67–84.

KULLENBERG, G. E. B. 1976. On vertical mixing and the energy transfer from the wind to the water. Tellus **28:** 159–165.

LEDWELL, J. R., AND A. BRATKOVICH. 1995. A tracer study of mixing in the Santa Cruz Basin. J. Geophys. Res. **100:** 20,681–20,704.

———, AND B. M. HICKEY. 1995. Evidence for enhanced mixing in the Santa Monica Basin. J. Geophys. Res. **100:** 20,665–20,679.

———, AND A. J. WATSON. 1991. The Santa Monica Basin tracer experiment: A study of diapycnical and isopycnical mixing. J. Geophys. Res. **96:** 8695–8718.

———, ———, AND C. S. LAW. 1993. Evidence for slow mixing across the pycnocline from an open-ocean tracer-release experiment. Nature **364:** 701–703.

LEMMIN, U. 1987. The structure and dynamics of internal waves in Baldeggersee. Limnol. Oceanogr. **32:** 43–61.

LOMBARDO, C. P., AND M. C. GREGG. 1989. Similarity scaling of viscous and thermal dissipation in a convecting surface boundary layer. J. Geophys. Res. **94:** 6273–6284.

MACINTYRE, S., K. M. FLYNN, R. JELLISON, AND J. R. ROMERO. 1999. Boundary mixing and nutrient flux in Mono Lake, California. Limnol. Oceanogr. **44:** 236–242.

MUNK, W. 1981. Internal waves and small scale processes, p. 264–291. *In* B. A. Warren and C. Wunsch [eds.], Evolution of physical oceanography. MIT Press, Cambridge.

MÜNNICH, M. 1996. The influence of bottom topography on internal seiches in stratified media. Dyn. Atmos. Oceans **23:** 257–266.

———, A. WÜEST, AND D. M. IMBODEN. 1992. Observations of the second vertical mode of the internal seiche in an alpine lake. Limnol. Oceanogr. **37:** 1705–1719.

OAKEY, N. S. 1982. Determination of the rate of dissipation of turbulent energy from simultaneous temperature and velocity shear microstructure measurements. J. Phys. Oceanogr. **12:** 256–271.

———, AND J. A. ELLIOTT. 1982. Dissipation within the surface mixed layer. J. Phys. Oceanogr. **12:** 171–185.

———, AND C. S. COX. 1972. Oceanic fine structure. Geophys. Fluid Dyn. **3:** 321–345.

OSBORN, T. R. 1980. Estimates of the local rate of vertical diffusion from dissipation measurements. J. Phys. Oceanogr. **10:** 83–89.

———, ———, AND J. M. TOOLE. 1988. On the parameterization of equatorial turbulence. J. Geophys. Res. **93:** 1199–1218.

PETERS, H., AND M. C. GREGG. 1988. Some dynamical and statistical properties of equatorial turbulence. p. 185–200. *In* J. C. J. Nihoul and B. M. Jamart [eds.], Small-scale turbulence and mixing in the ocean, Proceedings of the 19th International Colloquium on Ocean Hydrodynamics. Elsevier.

POWELL, T., AND A. JASSBY. 1974. The estimation of vertical eddy diffusivities below the thermocline in lakes. Water Resour. Res. **10:** 191–198.

RAVENS, T. M., O. KOCSIS, N. GRANIN, AND A. WÜEST. 2000. Small-scale turbulence and vertical mixing in Lake Baikal. Limnol. Oceanogr. **45:** 159–173.

ROHR, J. J., AND C. W. VAN ATTA. 1987. Mixing efficiency in stably stratified growing turbulence. J. Geophys. Res. **92:** 5481–5488.

SCHIMMELE, M. 1993. Anregung interner Seiches im Bodensee durch den Wind. Ph.D. Dissertation, Inst. Umweltphysik, Univ. of Heidelberg.

SCHLICHTING, H. 1968. Boundary-layer theory. McGraw-Hill.

SPIGEL, R. H., AND J. IMBERGER. 1980. The classification of mixed-layer dynamics in lakes of small to medium size. J. Phys. Oceanogr. **10:** 1104–1121.

STILLINGER, D. C., K. N. HELLAND, AND C. W. VAN ATTA. 1983. Experiments on the transition of homogeneous turbulence to internal waves in a stratified fluid. J. Fluid Mech. **131:** 91–122.

THORPE, S. A. 1977. Turbulence and mixing in a Scottish loch. Philos. Trans. R. Soc. Lond. A **286:** 125–181.

———. 1988. The dynamics of the boundary layers of the deep ocean. Sci. Prog. **72:** 189–206.

TOOLE, J. M., K. L. POLZIN, AND R. W. SCHMITT. 1994. Estimates of diapycnal mixing in the abyssal ocean. Science **264:** 1120–1123.

WU, J. 1994. The sea surface is aerodynamically rough even under light winds. Boundary-Layer Meteorol. **69:** 149–158.

WÜEST, A. 1987. Ursprung und Grösse von Mischungsprozessen im Hypolimnion natürlicher Seen. Ph.D. Dissertation, no. 8350, ETH, Zurich.

———, AND M. GLOOR. 1998. Bottom boundary mixing: The role of near-sediment density stratification. *In* J. Imberger [ed.], Physical processes in lakes and oceans. Coastal Estuarine Stud. **54:** 464–480.

———, D. C. VAN SENDEN, J. IMBERGER, G. PIEPKE, AND M. GLOOR. 1996. Comparison of diapycnal diffusivities measured by tracer and microstructure techniques. Dyn. Atmos. Oceans **24:** 27–39.